

Radiative Penguin Decays

Jürgen Kroseberg
 Santa Cruz Institute for Particle Physics, University of California,
 1156 High Street, Santa Cruz, CA 95064, USA

Selected recent results from experimental studies of radiative penguin decays of B mesons by the Belle and BABAR collaborations are discussed: preliminary findings from a first inclusive measurement of $b \rightarrow s\gamma$ using a hadronic tag by BABAR, first presented at this conference, updated preliminary results Belle on $B \rightarrow p\bar{A}\gamma$, first shown at the Moriond QCD workshop earlier this year, and a recently published BABAR study of $B \rightarrow \rho\gamma$ and $B \rightarrow \omega\gamma$ decays.

1. Introduction

Within the standard model of particle physics (SM), the rare, flavor-changing-neutral-current decays $b \rightarrow d\gamma$ and $b \rightarrow s\gamma$ are forbidden at tree level. The leading-order processes are one-loop electroweak penguin diagrams as shown in Figure 1, where the top quark is the dominant virtual quark contribution. In the context of theories beyond the SM, new virtual particles may appear in the loop, which could lead to measurable effects on experimental observables such as branching fractions and CP asymmetries [1].

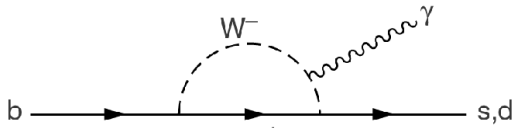


Figure 1: Example leading-order Feynman diagram for $b \rightarrow s\gamma$ and $b \rightarrow d\gamma$ transitions.

The shape of the photon energy spectrum is insensitive to non-SM physics [2] but can be used to determine the Heavy Quark Expansion (HQE) parameters M_{ES} and μ_π^2 , which are related to the mass and momentum of the b quark within the B meson. Improved measurements of these parameters are relevant to, e.g., reduce the error in the CKM matrix elements $|V_{cb}|$ and $|V_{ub}|$ determined from semi-leptonic B -meson decays [3].

In the following, three recent experimental studies of radiative penguin decays are discussed

2. Measuring $b \rightarrow s\gamma$ with a hadronic tag

Previous inclusive measurements of $b \rightarrow s\gamma$ transitions, by the CLEO [4], Belle [5] and BABAR [6, 7] collaborations, used either fully inclusive event samples, requiring only a high-energy lepton in the event or no tag at all, or a combination of several exclusive decay modes. A new (preliminary) analysis, based on BABAR data corresponding to an integrated luminosity of 210 fb^{-1} , uses for the first time a recoil method

to select candidate B decays, where $B\bar{B}$ events are tagged by a fully reconstructed hadronic decay of one the B mesons, in the following referred to as the *tag* B , and radiatively decaying *signal* B mesons are reconstructed from the remaining particles in the event. While the hadron tag efficiency is low (about 0.3%), this method allows for the inclusive study of $b \rightarrow s\gamma$ decays in a relatively clean environment and a determination of the momentum, charge, and flavor of the B mesons. Thus, it is possible to measure the photon spectrum in the rest frame of the signal B , to separate charged and neutral B mesons and to determine the CP -asymmetry A_{CP} .

In order to reconstruct a large sample of tag B mesons, hadronic decays to $\bar{D}Y^\pm$ and \bar{D}^*Y^\pm final states are selected, where Y^\pm denotes relevant combinations of mesons $-\pi^\pm, K^\pm, K_s^0$, and π^0 – with a total charge of ± 1 [8]. Those particles in the event that are not reconstructed as part of the tag B are required to include an isolated, well-reconstructed photon candidate with an energy $E_\gamma > 1.3 \text{ GeV}$ in the signal B meson rest frame. Photon candidates that are found to be consistent with stemming from π^0 or η decays are rejected. Continuum backgrounds ($e^+e^- \rightarrow q\bar{q}$, with $q = u, d, s, c$) are suppressed using a Fisher discriminant combining twelve quantities that are sensitive to event shape differences between B decays and continuum processes.

The numbers of remaining B and non- B events are determined by means of fits to the beam-energy-substituted mass $M_{ES} = \sqrt{s/4 - \vec{p}_B^2}$.¹ The left hand side of Figure 2 shows the preliminary results as a function of the photon energy. The points are from the data; the solid histogram was obtained from a $B\bar{B}$ Monte Carlo sample (excluding the signal decay $B \rightarrow X_s\gamma$) and then scaled according to the results of a fit to the data in the region $1.3 \text{ GeV} < E_\gamma < 1.9 \text{ GeV}$. For $E_\gamma > 1.9 \text{ GeV}$ 119 ± 22 $B \rightarrow X_s\gamma$ signal events are observed over a $B\bar{B}$ background of 145 ± 9 events.

The differential decay rate $(1/\Gamma_B)(d\Gamma/dE_\gamma)$ is mea-

¹Here, \sqrt{s} is the total energy in the center of mass (CM) frame, and \vec{p}_B denotes the B candidate CM momentum.

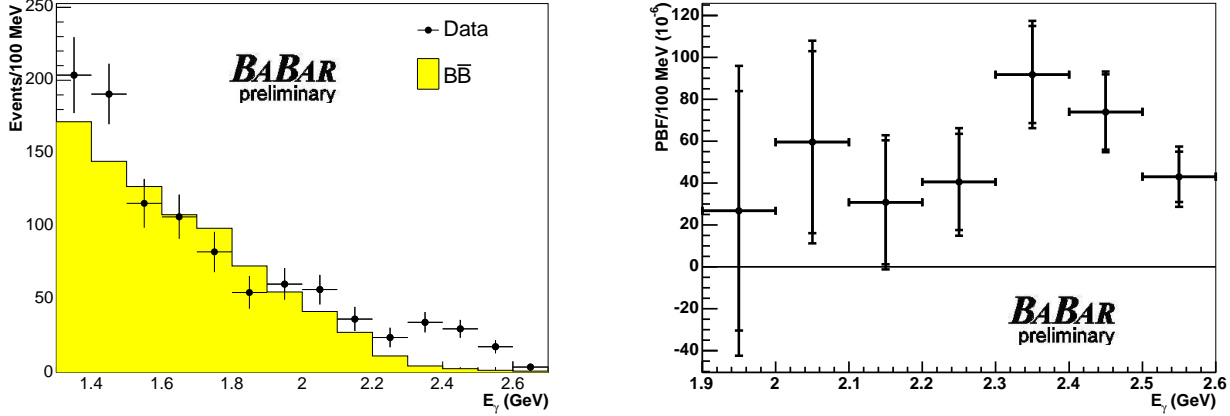


Figure 2: Left: the measured numbers of B events as a function of photon energy. The points are from data; the histogram is from a $B\bar{B}$ Monte Carlo sample which excludes the signal decay $B \rightarrow X_s\gamma$; Right: the partial branching fractions $(1/\Gamma_B)(d\Gamma/dE_\gamma)$ with statistical and total error. All results are preliminary

Table I Preliminary results for the $b \rightarrow s\gamma$ branching fraction and moments of the photon energy spectrum, with statistical and systematic errors, for different minimum photon energies E_{cut} .

E_{cut} (GeV)	$\mathcal{B}(B \rightarrow X_s\gamma)$ (10^{-6})	$\langle E_\gamma \rangle$ (GeV)	$\langle (E_\gamma - \langle E_\gamma \rangle)^2 \rangle$ (GeV^2)
1.9	$366 \pm 85 \pm 59$	$2.289 \pm 0.058 \pm 0.026$	$0.0334 \pm 0.0124 \pm 0.0263$
2.0	$339 \pm 64 \pm 47$	$2.315 \pm 0.036 \pm 0.020$	$0.0265 \pm 0.0057 \pm 0.0203$
2.1	$278 \pm 48 \pm 34$	$2.371 \pm 0.025 \pm 0.011$	$0.0142 \pm 0.0037 \pm 0.0111$
2.2	$248 \pm 38 \pm 26$	$2.398 \pm 0.016 \pm 0.006$	$0.0092 \pm 0.0015 \pm 0.0061$
2.3	$207 \pm 30 \pm 19$	$2.427 \pm 0.010 \pm 0.007$	$0.0059 \pm 0.0007 \pm 0.0073$

sured in bins of the signal B rest frame photon energy in the range $1.9 \leq E_\gamma < 2.6$ GeV. For a given bin i this is determined according to

$$\frac{1}{\Gamma_B} \frac{d\Gamma_i}{dE_\gamma} = \frac{N_i - b_i}{\varepsilon_i N_B C_{\text{tag}}}, \quad (1)$$

where N_i is the number of B events in the bin, b_i is the number of B mesons from decays other than $b \rightarrow (s, d)\gamma$, and N_B is the total number of B mesons in the sample. The efficiency ε_i corrects for both acceptance and bin-to-bin resolution effects, and the correction factor C_{tag} accounts for any dependence of the hadronic B tag probability on the the presence of a $B \rightarrow X_s\gamma$ final state.

In the right part of Figure 2 the partial branching fraction is shown after all corrections. The systematic uncertainties – mainly arising from the modelling of the $B\bar{B}$ background, the M_{ES} fit parametrization, the description of the detector response, and the dependence on the $B \rightarrow X_s\gamma$ signal model – are included here. The results for the integrated branching fraction and moments of the photon energy spectrum above different minimum photon energies E_{cut} are summa-

rized in Table I. Figure 3 shows the first and second moments of the photon energy spectrum as a function of E_{cut} ; good agreement with previous measurements is found.

Using [3] to extrapolate the measured branching fraction down to a minimum photon energy of 1.6 GeV yields

$$\mathcal{B}(b \rightarrow s\gamma)|_{E_\gamma > 1.6 \text{ GeV}} = (3.9 \pm 0.9 \pm 0.6) \times 10^{-4}. \quad (2)$$

This is in good agreement with the current experimental world average [12] of $(3.55 \pm 0.26) \times 10^{-4}$ as well as recent NNLO QCD calculations [9–11].

All these preliminary results are currently limited by statistics; adding more data in future measurements is expected to significantly reduce also the systematic uncertainties. It should also be noted that the recoil method is complementary to those of other measurements of $b \rightarrow s\gamma$ transitions; the largely independent systematic uncertainties will facilitate a combination of the results.

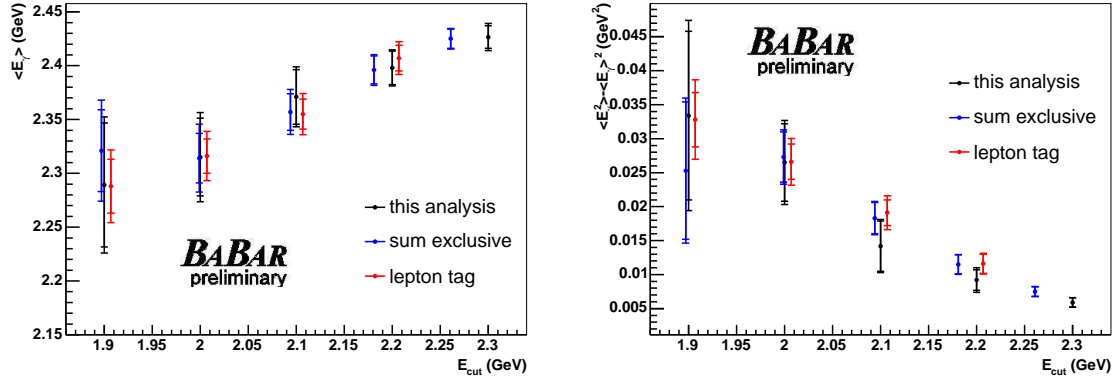


Figure 3: First and second moments of the photon energy spectrum as a function of E_{cut} . For comparison, the results from [6] and [7] are shown as well.

3. Study of $B \rightarrow p\bar{\Lambda}\gamma$ decays

The decay $B^+ \rightarrow p\bar{\Lambda}\gamma$ was first observed by Belle in 2005 based on a data sample corresponding to an integrated luminosity of 140 fb^{-1} [13]. These results have now been updated with a preliminary measurement² using 414 fb^{-1} of Belle data. This is a rare process; the SM branching fraction is predicted to be $\approx 1 \times 10^{-6}$. The final state baryons restrict the phase space, thus giving access to low photon momenta. The experimental study of this decay provides information on the baryon production mechanism. For example, the spin of the s quark can be probed through a helicity analysis; large wrong-helicity contributions would indicate physics beyond the SM.

Figure 4 shows the projections of a two-dimensional

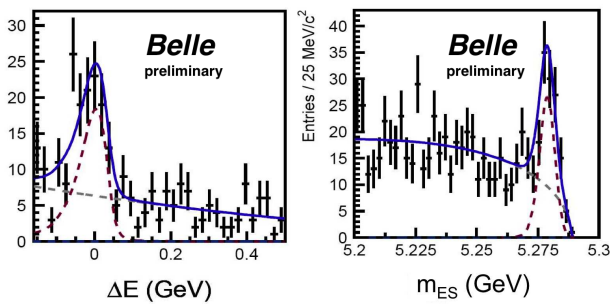


Figure 4: The ΔE (left) and M_{ES} (right) distributions for selected $B^+ \rightarrow p\bar{\Lambda}\gamma$ in the $p\bar{\Lambda}$ invariant mass region $< 2.8 \text{ GeV}$, together with the result of the fit (solid curve), which is also shown separated into signal (dash-dotted) and background (dashed) components.

²Since this conference, this analysis has been finalized and published [16].

fit to the distributions of the energy difference $\Delta E \equiv E_B^* - E_{\text{beam}}^*$, where E_B^* is the CM energy of the B meson candidate and E_{beam}^* is the CM beam energy, and M_{ES} for selected events with an invariant di-baryon mass $m_{p\bar{\Lambda}} < 2.8 \text{ GeV}$. About 100 signal events are found, corresponding to a statistical significance of 14σ . Turning this into a branching fraction and extrapolating to the full di-baryon mass range yields

$$\mathcal{B} = (2.45^{+0.44}_{-0.38} \pm 0.22) \times 10^{-6}, \quad (3)$$

somewhat above current SM predictions [14, 15].

A near-threshold enhancement is found in the di-baryon mass distribution, see the left part of Figure 5. This was previously observed for other baryonic B de-

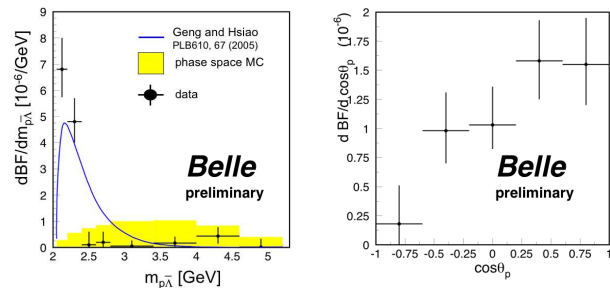


Figure 5: Measured distributions of the $p\bar{\Lambda}$ invariant mass (left), compared to theoretical expectations, and $\cos(\theta_p)$, where the helicity angle θ_p is the angle between proton and photon direction in the di-baryon rest frame.

cays and has since then been the focus of considerable theoretical interest.

The right hand side of Figure 5 shows the measured distribution of $\cos(\theta_p)$, where the helicity angle θ_p is the angle between proton and photon direction in the di-baryon rest frame. It is consistent with a short-distance $b \rightarrow s\gamma$ description of this decay. The asymmetry with respect to $\cos(\theta_p) = 0$ is

Table II Measured branching fractions \mathcal{B} , angular asymmetries A_θ , and CP asymmetries A_{CP} . All results are preliminary.

Mode	\mathcal{B} (10^{-6})	A_θ	A_{CP}
$B^+ \rightarrow p\bar{A}\gamma$	$2.45^{+0.44}_{-0.38} \pm 0.22$	$+0.29 \pm 0.14$	$+0.17 \pm 0.17$
$B^+ \rightarrow p\bar{A}\pi^0$	$3.00^{+0.61}_{-0.53} \pm 0.33$	-0.16 ± 0.18	$+0.01 \pm 0.17$
$B^0 \rightarrow p\bar{A}\pi^-$	$3.23^{+0.33}_{-0.29} \pm 0.29$	-0.41 ± 0.11	-0.02 ± 0.10

determined to be $A_\theta = 0.29 \pm 0.14$. The CP asymmetry, $A_{CP} = 0.17 \pm 0.17$, is found to be consistent with zero.

Table II summarizes these results and includes, for comparison, corresponding measurements for the decays $B^+ \rightarrow p\bar{A}\pi^0$, which is observed for the first time, and $B^0 \rightarrow p\bar{A}\pi^-$.

4. $B \rightarrow \rho/\omega\gamma$ branching fractions

With respect to $b \rightarrow s\gamma$, the corresponding $b \rightarrow d\gamma$ branching fractions are suppressed by a factor ≈ 0.04 ; the SM branching fractions for the decays of B mesons to $\rho\gamma$ and $\omega\gamma$ are $\mathcal{O}(10^{-6})$. While the calculations of the exclusive decay rates have large uncertainties due to non-perturbative long-distance QCD effects, some of this uncertainty cancels in the ratio of $B \rightarrow \rho/\omega\gamma$ to $B \rightarrow K^*\gamma$ branching fractions. Since the dominant diagram involves a virtual top quark, this ratio is related to the ratio of Cabibbo-Kobayashi-Maskawa (CKM) matrix elements $|V_{td}/V_{ts}|$ [17, 19, 28] via³

$$\frac{\mathcal{B}[B \rightarrow (\rho/\omega)\gamma]}{\mathcal{B}(B \rightarrow K^*\gamma)} = \left| \frac{V_{td}}{V_{ts}} \right|^2 \left(\frac{1 - m_\rho^2/M_B^2}{1 - m_{K^*}^2/M_B^2} \right)^3 \zeta^2 [1 + \Delta R]. \quad (4)$$

Physics beyond the Standard Model could affect these decays, creating inconsistencies between this measurement of $|V_{td}/V_{ts}|$ and that obtained from the ratio of B^0 and B_s^0 mixing frequencies [20].

After previous searches by BABAR [21] and CLEO [22], which found no evidence for the decays $B \rightarrow \rho\gamma$ and $B \rightarrow \omega\gamma$, an observation of the decay $B^0 \rightarrow \rho^0\gamma$ was reported by the Belle collaboration [23]. A recently published BABAR study [24] of the decays $B^+ \rightarrow \rho^+\gamma$, $B^0 \rightarrow \rho^0\gamma$, and $B^0 \rightarrow \omega\gamma$ is summarized in the following.

From a data sample containing 347 million $B\bar{B}$ pairs, which corresponds to an integrated luminosity of 316 fb^{-1} , the decays $B \rightarrow \rho\gamma$ and $B \rightarrow \omega\gamma$ are reconstructed by combining a high-energy photon

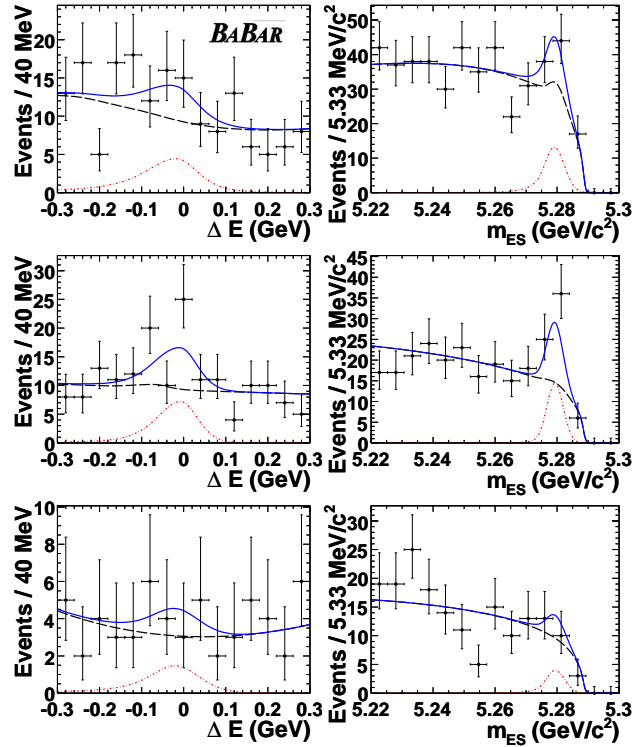


Figure 6: ΔE and M_{ES} projections of the fits for the decay modes $B^+ \rightarrow \rho^+\gamma$ (top), $B^0 \rightarrow \rho^0\gamma$ (middle), and $B^0 \rightarrow \omega\gamma$ (bottom). In each plot, the signal fraction is enhanced by selections on the other fit variables. The points are data, the solid line is the total of all contributions, and the long-dashed (dashed-dotted) line is background-only (signal-only).

with a vector meson reconstructed in the decay modes $\rho^0 \rightarrow \pi^+\pi^-$, $\rho^+ \rightarrow \pi^+\pi^0$, and $\omega \rightarrow \pi^+\pi^-\pi^0$. The dominant source of background is continuum events ($e^+e^- \rightarrow q\bar{q}$, with $q = u, d, s, c$) that contain a high-energy photon from π^0 or η decays. Other backgrounds include photons from initial-state radiation processes, decays of $B \rightarrow K^*\gamma$ ($K^* \rightarrow K\pi$), decays of $B \rightarrow (\rho/\omega)\pi^0$ or $B \rightarrow (\rho/\omega)\eta$ and combinatorial background from higher-multiplicity $b \rightarrow s\gamma$ decays.

High-energy photons γ for which the combination with another photon γ' is found – based on a likelihood ratio constructed from $E_{\gamma'}$ and $m_{\gamma\gamma'}$ – to be consistent with a π^0 or η decay are rejected. A neural network, exploiting differences between background and B decays in, e.g., lepton and kaon production (through flavor-tagging variables described in [25]) and event shape, is used to suppress continuum background events.

The signal content of the data is determined by a multidimensional unbinned maximum likelihood fit, which is constructed individually for each of the three

³The coefficient ζ is the ratio of the form factors for the decays $B \rightarrow \rho\gamma$ and $B \rightarrow K^*\gamma$ and ΔR accounts for different dynamics in the decay.

Table III The signal yield (n_{sig}), significance (Σ) in standard deviations including systematic errors, efficiency (ϵ), and branching fraction (\mathcal{B}) for each mode. The errors on n_{sig} are statistical only, while for the branching fraction the first error is statistical and the second systematic.

Mode	BABAR			Belle		
	n_{sig}	Σ	$\mathcal{B}(10^{-6})$	n_{sig}	Σ	$\mathcal{B}(10^{-6})$
$B^+ \rightarrow \rho^+ \gamma$	$42.0^{+14.0}_{-12.7}$	3.8σ	$1.10^{+0.37}_{-0.33} \pm 0.09$	8.5	1.6σ	$0.55^{+0.42+0.09}_{-0.36-0.08}$
$B^0 \rightarrow \rho^0 \gamma$	$38.7^{+10.6}_{-9.8}$	4.9σ	$0.79^{+0.22}_{-0.20} \pm 0.06$	20.7	5.2σ	$1.25^{+0.37+0.07}_{-0.33-0.06}$
$B^0 \rightarrow \omega \gamma$	$11.0^{+6.7}_{-5.6}$	2.2σ	$0.40^{+0.24}_{-0.20} \pm 0.05$	5.7	2.3σ	$0.56^{+0.34+0.05}_{-0.27-0.10}$
$B \rightarrow (\rho/\omega)\gamma$		6.4σ	$1.25^{+0.25}_{-0.24} \pm 0.09$	36.9	5.1σ	$1.32^{+0.34+0.10}_{-0.31-0.09}$
$B \rightarrow \rho \gamma$		6.0σ	$1.36^{+0.29}_{-0.27} \pm 0.10$			

signal decay modes. All fits use ΔE , M_{ES} , $\cos\theta_H$,⁴ and the neural network output N . For decays $B^0 \rightarrow \omega\gamma$ ($\omega \rightarrow \pi^+\pi^-\pi^0$), the cosine of the angle between the π^+ and π^0 momenta in the $\pi^+\pi^-$ rest frame (Dalitz angle) is added as a fifth observable. In the fit, signal, continuum background, $B \rightarrow K^*\gamma$ decays, and other B backgrounds are considered as hypotheses for the origin of the events.

Figure 6 shows the data points and the projections of the fit results for ΔE and M_{ES} separately for each decay mode. The signal yields and corresponding branching fractions are listed in Table III.

The isospin symmetry is tested by measuring the quantity $\Gamma(B^+ \rightarrow \rho^+\gamma)/[2\Gamma(B^0 \rightarrow \rho^0\gamma)] - 1 = -0.35 \pm 0.27$, which – within the large uncertainties – agrees with the theoretical expectation [17]. The measured branching fractions are consistent with the isospin relation $\Gamma_{B \rightarrow \rho^+\gamma} = 2\Gamma_{B \rightarrow \rho^0\gamma} = 2\Gamma_{B \rightarrow \omega\gamma}$ among the widths of the individual decays. Imposing this relation as a constraint, the isospin-averaged branching fraction is determined from a simultaneous fit to the three decay modes to be

$$\mathcal{B}[B \rightarrow (\rho/\omega)\gamma] = (1.25^{+0.25}_{-0.24} \pm 0.09) \times 10^{-6}; \quad (5)$$

the significance of the signal is 6.4σ , including systematic uncertainties. Excluding the $B^0 \rightarrow \omega\gamma$ mode from the simultaneous fit yields $\mathcal{B}(B \rightarrow \rho\gamma) = (1.36^{+0.29}_{-0.27} \pm 0.10) \times 10^{-6}$.

As shown in Table III and Figure 7, all these results agree well with corresponding measurements by the Belle collaboration, published in [23].⁵

⁴The helicity angle θ_H is defined as the angle between the B momentum vector and the π^- track calculated in the ρ rest frame in the case of a ρ meson, or the angle between the B momentum vector and the normal to the ω decay plane for an ω meson.

⁵It should be noted that since this conference Belle has reported updated results based on a significantly larger dataset ($\approx 600 \text{ fb}^{-1}$). Good agreement with the previous measurements is found; still no significant signal is seen for the decay $B^0 \rightarrow \omega\gamma$. Details can be found in [26].

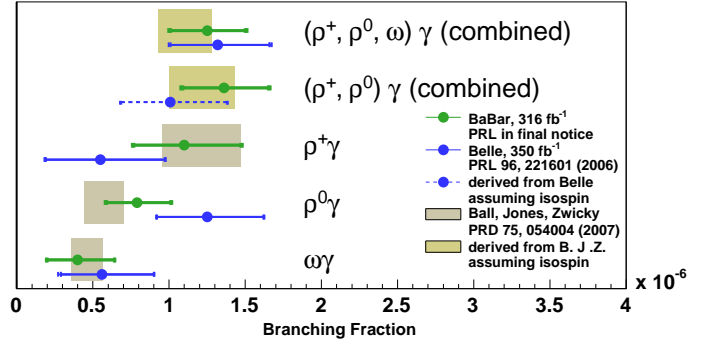


Figure 7: Measured $B \rightarrow \rho\gamma$ and $B \rightarrow \omega\gamma$ branching fraction, compared to theoretical predictions.

Using the world average value of $\mathcal{B}(B \rightarrow K^*\gamma)$, Equation (4), and theory input from [27], this translates into

$$|V_{td}/V_{ts}| = 0.200^{+0.021}_{-0.020} \pm 0.015, \quad (6)$$

where the first error is experimental and the second is theoretical. This result is in very good agreement with the measurement of this ratio from the study of B^0 and B_s^0 mixing [20].

Acknowledgments

Thanks to the FPCP2007 organizers for making this productive and enjoyable conference possible.

References

- [1] See, for example, S. Bertolini, F. Borzumati, and A. Masiero, Nucl. Phys. B **294**, 321 (1987); H. Baer and M. Brhlik, Phys. Rev. D **55**, 3201 (1997); J. Hewett and J. Wells, Phys. Rev. D **55**, 5549 (1997); M. Carena *et al.*, Phys. Lett. B **499**, 141 (2001).

- [2] A. L. Kagan and M. Neubert, *Eur. Phys. Jour. C* **7**, 5 (1999).
- [3] O. Buchmüller and H. Flächer, *Phys. Rev. D* **73**, 073008 (2006).
- [4] S. Chen *et al.* [CLEO Collaboration], *Phys. Rev. Lett.* **87**, 251807 (2001).
- [5] P. Koppenburg *et al.* [Belle Collaboration], *Phys. Rev. Lett.* **93**, 061803 (2004).
- [6] B. Aubert *et al.* [BABAR Collaboration], *Phys. Rev. D* **72**, 052004 (2005).
- [7] B. Aubert *et al.* [BABAR Collaboration], *Phys. Rev. Lett.* **97**, 171803 (2006).
- [8] B. Aubert *et al.* [BABAR Collaboration], *Phys. Rev. Lett.* **92**, 071802 (2004).
- [9] M. Misiak *et al.*, *Phys. Rev. Lett.* **98**, 022002 (2007).
- [10] T. Becher and M. Neubert, *Phys. Lett. B* **637**, 251 (2006).
- [11] J. Andersen and E. Gardi, *JHEP* **01**, 029 (2007).
- [12] Heavy Flavor Averaging Group, hep-ex/0603003.
- [13] Y. J. Lee *et al.* [Belle Collaboration], *Phys. Rev. Lett.* **95**, 061802 (2005).
- [14] H. Y. Cheng and K. C. Yang, *Phys. Lett. B* **533**, 271 (2002).
- [15] C. Q. Geng and Y. K. Hsiao, *Phys. Lett. B* **610**, 67 (2005).
- [16] M. Z. Wang *et al.* [Belle Collaboration], *Phys. Rev. D* **76**, 052004 (2007).
- [17] A. Ali, E. Lunghi, and A. Y. Parkhomenko, *Phys. Lett. B* **595**, 323 (2004).
- [18] S. W. Bosch and G. Buchalla, *Nucl. Phys. B* **621**, 459 (2002).
- [19] A. Ali and A. Y. Parkhomenko, *Eur. Phys. Jour. C* **23**, 89 (2002).
- [20] A. Abulencia *et al.*, *Phys. Rev. Lett.* **97**, 242003 (2006).
- [21] B. Aubert *et al.* [BABAR Collaboration], *Phys. Rev. Lett.* **94**, 011801 (2005).
- [22] T. E. Coan *et al.* [CLEO Collaboration], *Phys. Rev. Lett.* **84**, 5283 (2000).
- [23] D. Mohapatra *et al.*, [Belle Collaboration], *Phys. Rev. Lett.* **96**, 221601 (2006).
- [24] B. Aubert *et al.* [BABAR Collaboration], *Phys. Rev. Lett.* **98**, 151802 (2007).
- [25] B. Aubert *et al.*, *Phys. Rev. Lett.* **89**, 201802 (2002).
- [26] B. Nakao, *Probing New Physics with rare B decays*, presentation at Lepton-Photon 2007, http://chep.knu.ac.kr/lp07/htm/S7/S07_21.pdf.
- [27] P. Ball and R. Zwicky, *JHEP* **0604**, 046 (2006); P. Ball, G. Jones, R. Zwicky, *Phys. Rev. D* **75**, 054004 (2007).
- [28] S. W. Bosch and G. Buchalla, *JHEP* **0501**, 035 (2005).